

Carbon Accumulation in Mediterranean Rhodolith Beds during the Holocene

Silvia de Juan¹, Ryan Smazal², Claudio Lo Iacono³, Maria del Mar Gil¹, Andrea Cabrito³, Andres Ospina-Alvarez¹, Jorge Guillén³, Grace M. Cott², Laia Illa-López¹, Hilmar Hinz¹, Francesc Maynou³

¹Instituto Mediterráneo de Estudios Avanzados IMEDEA (UIB-CSIC), c. Miquel Marquès 21, 07190 – Esporles (Spain)

²School of Biology and Environmental Science, University College Dublin, Dublin, Ireland

³Institut de Ciències del Mar (CSIC), Psg. Marítim de la Barceloneta 37-49, 08003-Barcelona (Spain)

Correspondence to: Silvia de Juan, silvia.dejuan@csic.es

Abstract. Rhodolith and maërl beds are globally relevant biogenic ecosystems whose long-term carbon storage capacity remains poorly quantified, particularly in the Mediterranean. To fill this gap, we investigated the formation, structure, and carbon content of a sediment deposit underlying a rhodolith bed in the Menorca Channel (Western Mediterranean). High-resolution seismo-acoustic profiling revealed a highly heterogeneous biogenic sedimentary deposit at ~60 m depth, with thickness ranging from a few centimeters to 3.7 m (mean = 0.95 m). Seven cores extracted from the thickest sediment deposits were analyzed for grain size, carbonate content, bioclast composition, organic carbon, and radiocarbon age. Radiocarbon dating indicates that sediment accumulation began during the early Holocene (11,700–9,000 yr BP), when post-glacial sea-level rise transitioned the area from subaerial exposure to shallow-marine conditions. Despite the spatial limitation of collected data, several conclusions could be drawn. Early deposits produced during the last sea-level rise were dominated by bivalves and dispersed coralline fragments. The following establishment of modern sea level around 7,000–6,500 yr BP marks a change to the development of more stable dense rhodolith–maërl facies that persist today. Sediment accretion rates are low (median = 8.54 cm kyr⁻¹), reflecting very low external sediment supply, and slow growth of coralline algae. Organic carbon content in the upper 50 cm, representing the most dynamic and recently deposited carbon pool, averaged 0.57% (± 0.22), with an estimated organic carbon stock of 32.04 (± 4.18) Mg C ha⁻¹. These results show that rhodolith beds can act as long-term organic carbon stores, forming spatially complex Holocene deposits that have been largely overlooked.

Deleted: Millennial-Scale

Deleted: Deposits

Formatted: English (UK)

Formatted: Italian

Formatted: Spanish

Formatted: Spanish

Deleted: habitats

Deleted: vibro

Deleted: E

Deleted: were

Deleted: led

Deleted: Mediterranean

Deleted: whose contribution to carbon storage has

39 **Keywords**

40 Calcareous red algae; ~~sediment~~ organic carbon; organic carbon ~~sequestration~~; ~~Holocene deposits~~;
41 ~~paleoecology~~; Mediterranean Sea.

42 **Highlights**

- 43 • Seismo-acoustic mapping of a deep rhodolith deposit ~~revealed highly variable thickness~~.
- 44 • Holocene sedimentation began 11,700–9,000 yr BP during post-glacial sea-level rise.
- 45 • Dense rhodolith–maërl facies formed after sea-level stabilization ~7,000 yr BP.
- 46 • Accretion rates are low (8.54 cm kyr⁻¹), very low external sediment supply and slow algal growth.
- 47 • Organic carbon averages 32.04 (± 4.18) Mg C ha⁻¹ in the upper 50 cm, ~~of sediment~~.

48

49

50

Deleted: S

Deleted: sink

Deleted: Holocene; Radiocarbon dating

Deleted: s

Deleted: evidencing long-term carbon storage

56 1. INTRODUCTION

57 Marine ecosystems play an important role in the global carbon cycle by contributing to organic and in-
58 organic carbon storage. Coastal systems sequester atmospheric carbon dioxide (CO₂) through photosyn-
59 thesis and the subsequent burial of sedimentary organic carbon (Nellemann and Corcoran, 2009; Barbier
60 et al., 2011). Current evidence suggests that net organic carbon burial in the marine environment comes
61 from vegetated ecosystems such as mangroves, seagrass meadows and saltmarshes (Macreadie et al.,
62 2019). In contrast, calcifying algal systems such as rhodolith and maërl beds have received considerably
63 less attention, despite their global distribution and the millennial persistence of their deposits. These
64 characteristics suggests that they may represent an important, yet poorly quantified, long-term carbon
65 store (Aguirre et al., 2017; Tuya et al., 2023; Van der Heijden and Kamenos, 2015).

66 Rhodolith and maërl beds consist of free-living, non-geniculate calcareous red algae (Rhodophyta: Cor-
67 allinophycidae) that form multi-specific assemblages in subtidal environments. These habitats typically
68 occur on coarse mobile sediments under moderate hydrodynamic conditions that prevent burial while
69 maintaining sufficient irradiance (Aguirre et al., 2017; Basso et al., 2017; Bosence, 1983). Despite their
70 slow individual annual growth rates (~1 mm yr⁻¹), rhodolith accumulations can reach several meters in
71 thickness over hundreds to thousands of years. Living rhodoliths are restricted to the upper few centime-
72 ters of the bed, overlying deposits of fragmented coralline algae and skeletal remains of bryozoans, mol-
73 luscs, and echinoderms (Fornós and Ahr, 1997; Betzler et al., 2011; Mao et al., 2020).

74 These long-lived carbonate-rich deposits may store carbon through both the accumulation of biogenic
75 sediments and the trapping of organic carbon supplied from external sources (Mao et al., 2020; Schubert
76 et al., 2024). The high particle-trapping capacity of rhodolith beds, driven by the three-dimensional struc-
77 tural complexity of the algae, is a key mechanism underpinning this process (Mao et al., 2020; James et
78 al., 2024; Bulleri et al., 2025). This structure enhances the retention of suspended material, promoting
79 the accumulation of organic material and supporting carbon cycling within detritus-based food-webs
80 (Rendina et al., 2026). However, the broader role of rhodolith beds in carbon cycling remains uncertain,
81 as carbon storage through particle retention simultaneously occurs with calcium carbonate production, a
82 process that releases CO₂ (James et al., 2024a; Mao et al., 2024). Thus, in carbonate-dominated systems,
83 the balance between carbon burial and release of CO₂ is complex and not yet fully resolved (Macreadie
84 et al., 2019). For the purposes of this study, we focus specifically on quantifying sedimentary organic
85 carbon stocks and highlighting the potential for long-term storage, rather than resolving net ecosystem
86 carbon balance.

- Deleted: habitats
- Deleted:
- Deleted: ;
- Deleted: Most
- Deleted: Current knowledge
- Deleted: The c
- Deleted: how
- Deleted: of
- Deleted: mainly derives in the coastal ocean comess
- Deleted: ,
- Deleted: (Tuya et al., 2023)
- Deleted: .
- Deleted:
- Deleted: These systems are globally distributed and the ... [1]
- Deleted: (Aguirre et al., 2017)
- Deleted: ¶
- Deleted: Unlike typical blue carbon habitats, rhodolith ... [2]
- Formatted: Hyphenate
- Deleted: occurring as
- Moved down [1]: They occur from shallow to mesophotic
- Formatted: English (UK)
- Deleted: , with
- Deleted: Betzler et al., 2011;
- Deleted: .
- Deleted: (Mao et al., 2020).
- Deleted: ¶
- Formatted: French
- Formatted: French
- Moved up [2]: (Mao et al., 2020).
- Deleted: Rhodolith and maërl beds have the capacity to
- Deleted: In contrast to other well-known blue carbon h... [3]
- Formatted: French
- Deleted: ; James et al., 2024; Mao et al., 2020
- Deleted: (James et al., 2024; Bulleri et al., 2024; Mao ... [4]
- Deleted: co-occurs
- Deleted: is whether they are a long term store of carbon... [5]
- Deleted: ecosystems
- Deleted: For
- Deleted: I
- Deleted: driven by carbonates
- Deleted: I
- Commented [GC7]: I think this is good and should be ... [6]
- Deleted: However, empirical data on sediment organic ... [7]

257 Large rhodolith and maërl beds are present on modern and ancient carbonate shelves **across tropical to**
258 **polar regions (Riosmena-Rodríguez et al., 2017; Tuya et al., 2023)**, including the world's largest bed on
259 the Brazilian continental shelf (21 000 km², Amado-Filho et al., 2012). The Mediterranean hosts the
260 second-largest bed described to date, covering approximately 470 km² in the Menorca Channel, western
261 Mediterranean (Tabone et al., 2024). Its development has been facilitated by the clear waters and low
262 sediment input that characterize Mediterranean islands, allowing rhodolith beds to extend down to 90 m
263 depth (Joher et al., 2016). **Despite their ecological importance, the capacity of Mediterranean rhodolith**
264 **beds to store sedimentary organic carbon over centennial to millennial timescales remains poorly**
265 **quantified. This is particularly true for the vertical distribution and spatial variability of carbon stocks,**
266 **as well as their relationship with deposit accretion history,**
267 **This knowledge gap is especially relevant given the high vulnerability of rhodolith beds to disturbance**
268 **due to their slow growth and limited recovery capacity. These habitats are threatened by bottom-contact**
269 **fishing gears, elevated suspended sediments, and the cumulative effects of ocean warming and**
270 **acidification under climate change (Tuya et al., 2023; Trégarot et al., 2024). Although Mediterranean**
271 **rhodolith beds are protected under EU Regulation 1997/2006, the EU Habitats Directive, and the**
272 **UNEP/MAP Action Plan (2008), effective management remains limited due to insufficient spatial**
273 **coverage and ecological data. Improving knowledge of their organic carbon storage capacity is essential**
274 **not only to clarify their contribution to the global carbon cycle, but also to strengthen the scientific basis**
275 **for conservation (de Macêdo Carneiro et al., 2021; Schubert et al., 2024).**
276 This study quantifies the role of Mediterranean rhodolith beds in long-term organic carbon storage by
277 analyzing sedimentary organic carbon deposition of a well-preserved deposit in the Menorca Channel
278 (western Mediterranean). The Menorca Channel is a temperate carbonate shelf where rhodolith sediments
279 have accumulated since the early Holocene, providing a unique archive to examine carbon storage over
280 millennial timescales. Using high-resolution seismo-acoustic data, sediment cores and radiocarbon
281 dating, we estimate the stock of organic carbon in the upper 50 cm of sediments. We test the hypothesis
282 that this rhodolith bed represents a consistent Holocene carbon store, shaped by local environmental
283 conditions and long-term sea-level changes, with implications for regional protection schemes for these
284 habitats.

Deleted: They occur from shallow to mesophotic depths to polar regions (Riosmena-Rodríguez et al., 2017; Tuya et al., 2023).

Deleted: around the wor

Deleted: Id (Riosmena-Rodríguez et al., 2017),

Deleted: However,

Deleted: d

Deleted: functioning and carbon dynamics

Deleted: resolved

Deleted: ,

Deleted: regarding

Deleted: organic carbon accumulation

Deleted: ,

Deleted: small-scale spatial heterogeneity and

Deleted: long-term

Deleted: evolution of these deposits

Deleted: ¶

¶

¶

¶

¶

¶

¶

¶

¶

¶

¶

Deleted: ¶

Formatted: Not Highlight

349 **2. MATERIAL AND METHODS**

350 **2.1. Study area**

351 The Balearic continental shelf is a temperate, low-energy oligotrophic system dominated by carbonate-
352 producing habitats, including *Posidonia oceanica* meadows, coralligenous communities, and extensive
353 rhodolith–maërl beds (Canals and Ballesteros, 1997; [Betzler et al., 2011](#)). Our study focuses on the
354 Menorca Channel, a shallow carbonate platform (~100 m max depth) between Mallorca and Menorca,
355 where post-glacial neritic carbonates have accumulated since the early Holocene (Alonso et al., 1988;
356 [Betzler et al., 2011](#)). Rhodolith and maërl beds occur between 45–80 m depth on the platform (Fig. 1),
357 interspersed with detrital sands (de Juan et al., 2023). [The preservation of these environments](#) has been
358 [assisted](#) by a historical trawling exclusion zone surrounding nearby submarine cables and, more recently,
359 by the 2016 designation of the Menorca Channel as a Natura 2000 Site of Community Importance (SCI
360 ESZZ16002).

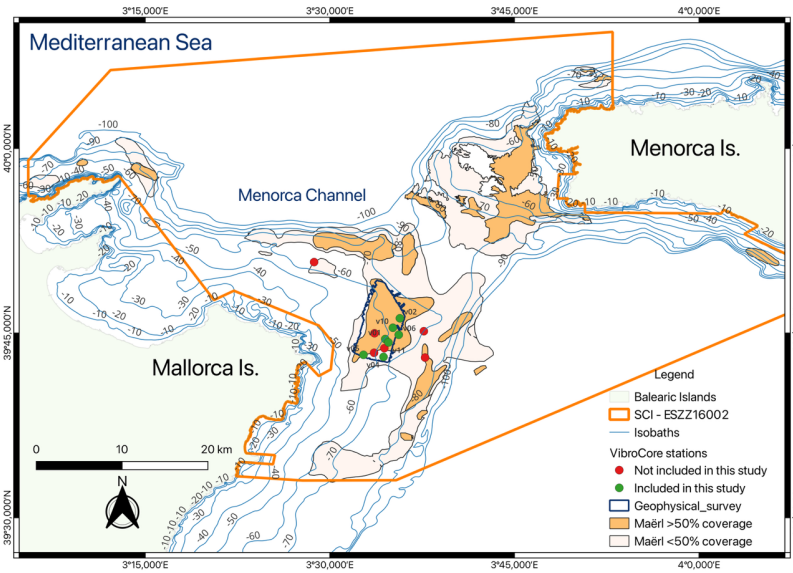
361 We focused on a 43.6 km² area where rhodolith and maërl cover exceeds 50%, based on high-resolution
362 mapping from the INDEMARES project (Moranta et al., 2014) and our own video surveys (Cabrito et
363 al., 2024b). Within this area, we conducted high-resolution seismo-acoustic profiling to determine the
364 thickness of bioclastic sediments above the acoustic basement and to identify suitable sites for recovering
365 ≥1-m sediment cores. Potential sites were inspected with a remotely operated vehicle (ROV) to confirm
366 rhodolith–maërl dominance, and full coverage was verified at all core locations.

Deleted: Betzler et al., 2011;

Deleted: and other macroalgae (*Laminaria rodriguezii*, *Osmundaria volubilis*, *Peyssonnelia rosamarina*) ...

Deleted: Habitat

Deleted: favored



373
 374 **Figure 1.** Study area in the Menorca Channel, located between Mallorca and Menorca islands in the western Mediterranean
 375 Sea. The map shows the area covered by the geophysical survey (dark blue polygon) and the location of VibroCore stations
 376 included (green dots) and not included (red dots) in this study. Rhodoliths are represented in light and dark orange,
 377 indicating areas with 10-50% and >50% coverage, respectively. The Site of Community Importance (SCI ESZZ16002) is
 378 delineated by the dark orange boundary. Isobaths (in metres) are shown as blue contour lines. Source: modified from project
 379 INDEMARES (Moranta et al., 2014).
 380

381 2.2. Geophysical map

382 In May 2022, we acquired 56 high-resolution seismo-acoustic profiles in the study area (Fig. 1) during a
 383 research cruise aboard R/V *SOCIB* and using an INNOMAR Medium-100 non-linear parametric
 384 echosounder coupled with an INS SBG Navisight Ekinox and GNSS AtlasLink for positioning. Sound-
 385 speed and turbidity corrections were obtained with a Valeport SWIFT. The system emits two primary
 386 frequencies around 100 kHz, producing a secondary frequency of 5–12 kHz, with a pulse repetition rate
 387 of up to 30 s⁻¹ and a beam width of ±1.8°. Non-linear parametric echosounders provide narrow, low-
 388 frequency beams with small footprints, enabling high-resolution imaging of shallow sediment deposits
 389 and precise localization of core-sampling (Lo Iacono et al., 2008).

390 Profiles were spaced 200 m apart, oriented NNE–SSW in the southern sector and NW–SE in the northern
 391 sector, intersected by perpendicular transversal profiles every 500–2000 m (Fig. A2.3). Penetration depth
 392 averaged 0.8–1.0 m and reached a maximum of 3.7 m, maintaining high horizontal and vertical metric
 393 to sub-metric resolution due to the small pulse size. Uncertainties were estimated to be of the order of ±

Deleted: targets

Deleted:

Deleted: supplementary material 1

Deleted: Measure u

Deleted: however

399 [0.2 m](#). Seismo-acoustic data were interpreted using INNOMAR-ISE 2.9 to pick stratigraphic horizons
 400 and estimate thickness of the bioclastic deposit. Geo-referencing and isopach mapping were conducted
 401 with Global Mapper and ArcGIS.

402 2.3. Sediment core sampling

403 In May 2023, sediment cores were collected at 60–80 m depth during a research cruise aboard
 404 R/V *Sarmiento de Gamboa*. [The coring sites](#) were selected based on geo-acoustic evidence of maximum
 405 sediment thickness within the survey polygon (Fig. 2). A vibrocorer (ASTHER I, GEOMYTSA S.A.)
 406 operating at 136 kN centrifugal force at 3 m recovered 12 PVC-lined cores (9 cm diameter, 1.4–2.8 m
 407 length; Table 1). Each core was sectioned into ≤1 m segments and stored at –20 °C for laboratory
 408 analyses. Of the 12 cores, 7 were retained for this study; [the remaining five cores were stored frozen for](#)
 409 [future genetic analysis to identify the presence of different species of rhodoliths](#) (Fig. 1).

410 **Table 1** – Characteristics of the seven vibrocores obtained in the Menorca Channel (Western Mediterranean) selected for
 411 this study. Description of biocenoses based on knowledge from our own video observations and previous projects ([Moranta](#)
 412 [et al., 2014](#)).

Vibrocore ID	Longitude	Latitude	Sea bottom Depth (m)	core length (m)	analyses	biocenose
V1	3.5750	39.7419	61.91	1.60	+ * #	rhodoliths >75%, with Peyssonnelia and Osmundaria
V2	3.5949	39.7700	66.22	1.40	+ * \$ #	rhodoliths >75%, with Laminaria
V4	3.5727	39.7177	66.08	1.80	+ * \$ #	rhodoliths >60%, with Osmundaria
V5	3.5456	39.7205	60.01	2.80	+ * #	rhodoliths >60%, with Osmundaria
V6	3.5933	39.7477	64.52	1.90	+ * \$ #	rhodoliths >60%, with Laminaria
V10	3.5854	39.7572	63.28	1.45	+ * #	rhodoliths >90%, with Peyssonnelia
V11	3.5794	39.7525	63.93	1.75	+ * \$ #	rhodoliths >75%, with Peyssonnelia

413 + Lithology and clasts composition; * Granulometry and carbonates; \$ Radiocarbon dating; # Organic carbon

414

415 Sediment core opening and visual description

416 Each 1 m core section was cut longitudinally for analysis. All cores were visually inspected to describe
 417 sediment composition, and subsamples were collected for grain size, radiocarbon dating, bioclast
 418 identification, and organic carbon content analyses.

419 Grain size and carbonate contents

420 The cores were sampled at 5 cm intervals for grain-size and carbonate-content analyses. Grain-size
 421 distributions were measured using a HORIBA LA-950V2 laser diffraction analyser after disaggregating
 422 and removing the biogenic fraction (10% H₂O₂), and ultrasonic dispersion; the >2 mm fraction was

Deleted: Cores' positions

Deleted:

Deleted: (projects MaCoBioS; MARBEFES)

Deleted: INDEMARES

Deleted: -

428 quantified by sieving. We calculated the weight percentages of clay, silt, sand, and gravel, as well as
429 mean grain size (ϕ), sorting (σ), skewness (Sk), and kurtosis (kG). Carbonate content was determined
430 from the CO₂ volume displaced by a sample of sediment treated with 20% HCl, calibrated against a 100%
431 CaCO₃ standard.

432 **Radiocarbon dating**

433 Between two and three bioclasts (rhodoliths or bivalve shells) from different depths in four cores (Table
434 1) were radiocarbon-dated by Beta Analytic (Miami, USA). Dates were calibrated with BetaCal 5.0, with
435 HPD method “MARINE20” and corrected for the local marine reservoir effect ($\Delta R = -112 \pm 99$).
436 Sediment accretion rates (cm kyr⁻¹) were calculated by dividing the thickness of sediment between
437 successive dated horizons along the core (kyr), taking the top most horizon as 0 yr BP.

438 **Taxonomic identification of bioclasts**

439 Sediment was examined under a binocular microscope at ~50 cm intervals for fauna identification.
440 Subsamples (10–20 g) were air-dried (48 h) and sieved through 0.5 and 1 mm meshes. Between 200 and
441 300 clasts from the >0.5–1 mm and >1 mm fractions were inspected and assigned to major taxonomic
442 groups (Bivalves, Gastropods, Bryozoans, Echinoids, Foraminiferans, and free-living coralline algae).
443 Rhodoliths were classified into two morphotypes following (Basso, 1998; Basso et al., 2012): non-
444 branched rhodoliths (including “boxwork” and “praline” forms; 1–5 cm) and branched maërl fragments
445 (0.5–2 cm) (see also Jardim et al., 2025; Teichert, 2024).

446 **2.4. Organic Carbon Content**

447 From each core, sediment samples (~21 ml) were collected using a syringe every 10 cm within the upper
448 50 cm, as this layer is expected to contain the highest and more dynamic carbon pool, which has not yet
449 undergone long-term diagenesis (Middelburg, 2018). To minimize decomposition of organic matter and
450 microbial growth, samples were kept cold (4 °C) during 24-48 [hours](#) for later processing. In the
451 laboratory, samples were weighed, freeze-dried (lyophilized) for 48-72 hours, and weighed again to
452 determine their moisture content percentage. Finally, the samples were finely ground in an agate ball
453 mill.

454 The processed samples were sent to University College Dublin to be sub-sampled for further analysis.
455 From each 10 cm layer, ~2.0 g (± 0.6 g) of homogenized sediment was subsampled for organic carbon
456 (OC) analysis. A sub-set of the homogenized sample was then shipped to the University of Waterloo
457 (Canada) for carbon and nitrogen analysis. The samples were analysed using an ECS 4010 Elemental

Deleted: subsequently

459 Analyzer (NC Technologies, Italy) coupled to a Delta Plus XL (Thermo-Finnegan, Germany) continuous
460 flow isotopic mass spectrometer (CRFIRMS). Samples were acid washed according to the University of
461 Waterloo Environmental Isotope Laboratory procedures in order to remove inorganic carbon and obtain
462 OC measurements. This included acid washing the sediments in HCl (10 ml of 10%) for 24 hours and
463 until the reaction subsided. The final OC value was determined using the measured OC percentage of the
464 acidified sample, which was normalized to the bulk sediment mass by multiplying by the samples non-
465 carbonate fraction. High effervescence during acid treatment indicated a substantial carbonate fraction,
466 resulting in a marked mass loss. The %C and %N was measured in bulk, analyzed against known certified
467 elemental standard materials. For QA/QC, sample replicates were analyzed every 8 to 10 samples, with
468 certified standard/reference materials comprising of at least 20% of every run. Analytical control
469 measures were based on the detection of major carbon (C) and nitrogen (N) peaks to ensure data
470 consistency and calibration accuracy.

471 2.5. Data analysis

472 To evaluate whether sediment characteristics control the density of retained OC, variation in OC density
473 (g/cm^3) was analysed in relation to sediment characteristics using linear mixed-effects models to account
474 for the hierarchical structure of the sampling design, with multiple depth subsamples collected within
475 each sediment core. Because OC density values were positive and right-skewed, the response was log-
476 transformed ($\log[\text{CarDens}]$) and modelled assuming Gaussian errors. Core identity was included as a
477 random intercept to accommodate non-independence among subsamples from the same core.

478 The following sediment characteristics, that were explored as candidate fixed effects, were: standardized
479 sediment depth (cm), median grain size (d_{50} ; μm), carbonate content (%), biogenic gravel content (%),
480 and sediment type (categorical). Owing to strong collinearity between d_{50} and the sand/silt fractions ($|r|$
481 $\approx 0.90\text{--}0.96$), grain-size fractions were not included in models containing d_{50} . Potential residual
482 dependence within each corer along the depth profile was assessed by fitting models with a first-order
483 autoregressive correlation structure, AR(1). In addition, a random-slope formulation allowing core-
484 specific depth trends was tested using a diagonal random-effects structure (random intercept and depth
485 slope by core, with intercept–slope covariance constrained to zero). Models were compared using Akaike
486 Information Criteria, with maximum likelihood estimation used for model selection and the best-
487 supported model refitted by restricted maximum likelihood for final parameter estimation. The intraclass
488 correlation coefficient (ICC) was calculated from variance components to quantify the proportion of
489 variance attributable to differences among cores. All analyses were conducted in R v4.4.2.

Deleted: organic carbon

Deleted:

Deleted:

Deleted:

Deleted: organic carbon

Deleted: organic carbon

Deleted: organic carbon

Deleted: within-core

Deleted: across depth

Deleted: evaluated

Deleted: an

Deleted: correlation structure along depth within each core

Deleted: c

503 **3. RESULTS**

504 **3.1. Seismoacoustic records**

505 The surveyed area ranges from 57 to 68 m depth and exhibits generally smooth bathymetry, with an
506 average slope of 0.2°. The western sector is relatively flat, gradually deepening from 57 to 60 m, while
507 the southeast and northeast sections show narrow bathymetric edges with steeper slopes reaching 68 m
508 (Fig. 2).

509 Geo-acoustic profiles allowed detailed mapping of the 3D architecture of the bioclastic deposit. Sediment
510 thickness was highly heterogeneous at small scales, ranging from nearly 0 to several meters over spatial
511 extents of hundreds of meters or less (Fig. 2, right panel; Fig. A1). Average thickness was 0.95 m, with a
512 maximum of 3.7 m. Thinner deposits occurred in the northern sector (down to 10 cm), whereas thicker
513 accumulations were found in the southern and eastern sectors, including a 2 km × 1 km patch reaching
514 3.7 m at its depocenter.

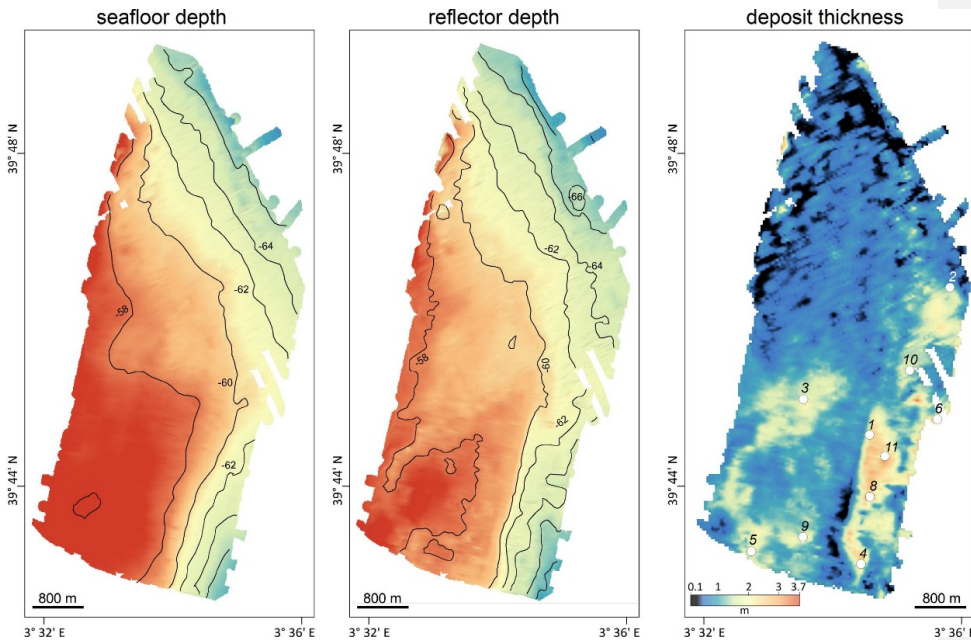
515 Cores were collected at locations of maximum sediment accumulation. Of the seven cores retained for
516 this study, V1, V2, and V10 reached the bedrock horizon; V4, V6, and V11 fell short by 0.5–1.1 m; and
517 V5 slightly penetrated the bedrock (~1 m) (Figs. 2 and 3; Fig. A1).

Deleted: supplementary

Deleted: material 1

Deleted: supplementary material 1

518



522
523 **Figure 2.** Results of the high-resolution profiling in the rhodolith deposit. Left panel: bathymetry, central panel: reflector
524 depth, right panel: deposit thickness. Refer to position of geophysical survey in Fig. 1.
525

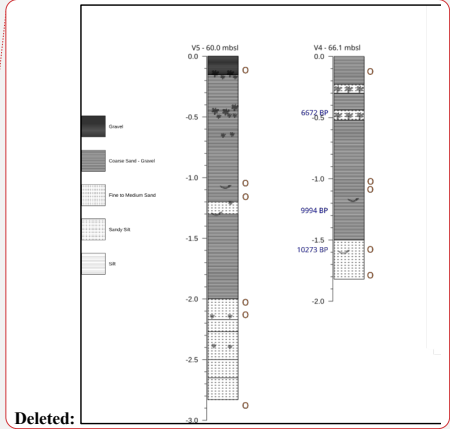
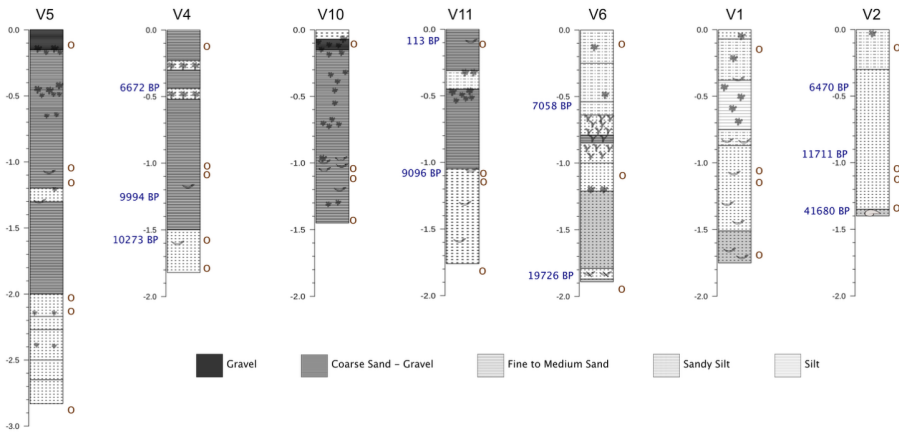
526 **3.2. Sediment characteristics**

527 Visual inspection of the cores revealed a relatively uniform composition, dominated by fine to coarse
528 bioclastic sand with occasional horizons of gravel or silt (Fig. 3; [Fig. A4](#)). Grain-size analysis confirmed
529 sand as the dominant fraction (>50%), with fines occasionally higher in certain horizons (e.g., V1: 40–
530 90 cm; V2: 30–60 cm; V4: 25–65 cm; V6: 25–60 cm; V11: 35–65cm), but never exceeding sand content.
531 Gravel was always <25%, with the exception of V5: 40–50 cm, 50% gravel. Carbonate contents were
532 consistently ≥90% along the cores.

533 Sediment composition was primarily carbonate bioclasts (75%) and, to a lesser extent, carbonate
534 lithoclasts (8%), with variable contributions from siliciclastic grains. Stereomicroscope analysis allowed
535 identification of 65% of clasts, mainly unattached coralline red algae (26%, branched and non-branched),
536 bivalve fragments (22%), gastropods (13%), echinoid remains (4%), foraminifera (4%), and bryozoans
537 (3%). Minor groups included serpulids, ostracods, and polyplacophorans. Siliciclastic grains (17%) were
538 grey or white lithoclasts, distinguished by texture and lack of reaction to dilute HCl.

539 Coralline algae fragments occurred throughout the cores, whereas well-formed rhodoliths were confined
540 to the upper ~60 cm (except V2), occurring either scattered or densely packed, particularly in V4, V5,
541 and V11 (Fig. 3). Three cores (V1, V2, V6) terminated on cemented substrate, including bivalve-rich
542 hardgrounds or reworked lithoclasts.

Deleted: supplementary material 2



544
545
546
547
548

Figure 3. Stratigraphic columns showing the lithological composition of the sediment and radiocarbon dates (in blue). Circles: sampling for faunistic identification: ○ Clasts (only clasts > 5 cm are represented): non-branched rhodolith: ○ branched rhodolith: Y entire bivalve shell: Y broken bivalve shell: Y rock fragment: Y

549 3.2.1. Radiocarbon Dating

550 Radiocarbon dating of rhodoliths and bivalve shells from four cores (Table 2) yielded ten age estimates.
551 Two basal ages (41,680 yr BP in V2 and 19,726 yr BP in V6) indicate reworked pre-Holocene material
552 from periods when the area was in an emerged sub-aerial setting. The next four oldest dates, between
553 11,711 and 9,096 yr BP, correspond to the end of Younger Dryas (11,711 yr BP) and the subsequent rapid
554 sea-level rise (until 9,000 yr BP), indicating that the area was a shallow marine environment (<20 m
555 depth) dominated by bivalves and dispersed branched rhodoliths. Some lithoclasts within these horizons
556 indicate continental input consistent with shallow-water conditions.

557 **Table 2.** Radiocarbon dates (¹⁴C) for carbonate bioclasts obtained from the testing laboratory of Beta Analytic (Miami, Fl.,
558 US), recalibrated with BetaCal 5.0 and corrected for the local marine reservoir effect (-112 ± 99). * correspond to reworked
559 ages

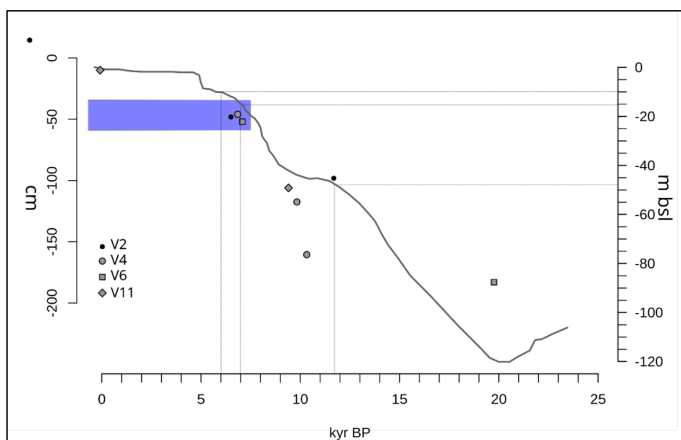
Core	Depth (cm)	Radiocarbon Date BP	Calibrated Probability Data (2 sigma)	Calibrated years BP
V2	136	37934 ± 875	41146-38315 BC 100%	41680.5*
V2	97	10490 ± 30	10151-9371 BC 95.4%	11711
V2	47	6110 ± 30	4778-4261 BC 95.4%	6470
V4	160.5	9460 ± 30	8640-8006 BC 95.4%	10273
V4	117.5	9270 ± 30	8372-7716 BC 95.4%	9994
V4	46	6300 ± 30	5000-4444 BC 95.4%	6672
V6	183	28067 ± 392	30634-4918 BC 100%	19726*

Formatted Table

Formatted Table

V6	52	6552 ± 81	5298–4918 BC 100%	7058
V11	106	8530 ± 30	7455–6837 BC 95.4%	9096
V11	10	340 ± 30	1724–1950 BD 95.4%	113

562
 563 Three younger ages, between 7,058 and 6,470 yr BP (47–52 cm depth in V2, V4, and V6), correspond to
 564 a period when the Menorca Channel was ~10–15 m below present sea level, during which well-formed,
 565 densely packed rhodoliths accumulated (Fig. 3). During this interval, continental inputs diminished,
 566 maërl became abundant, and rhodolith beds consolidated, as exemplified by V4 (~50 cm, 6,672 yr BP).
 567 Scattered rhodolith fragments occasionally occur at greater depths, but none are found in strata older than
 568 9,096 yr BP, highlighting the onset of persistent rhodolith accumulation after postglacial transgression.
 569 Based on these dates, sediment accretion rates range from 6.9 to 21.5 cm kyr⁻¹, with a median of 8.54
 570 cm kyr⁻¹ (Fig. 4).



571
 572
 573 **Figure 4.** Age-depth plot for the dated cores (excluding one sample that yielded a date > 40 ky BP) from the rhodolith
 574 deposit of the Menorca channel. Sea-level height (m) relative to present day based on the average model from (Bianchi et
 575 al., 2012), largely based on results from (Lambeck and Bard, 2000). Relevant dates for this deposit (end of Younger Dryas at
 576 11700 yr BP and period of sea level stabilization between 7000 and 6000 yr BP) are marked along the x-axis and the
 577 corresponding depth below current sea level on the right y-axis. Blue stripe between 35 and 60 cm core depth shows the
 578 onset of horizons with high abundance of rhodoliths.
 579

580 3.3. Organic Carbon content

581 The average OC content in the upper 50 cm of sediment across all cores was 0.57% (± 0.22) (Table 3).
 582 OC content showed little variation with depth within this interval (Table A1). Using these measurements,
 583 OC stocks were determined for each core. Over the first 30 cm, we estimate an average across all the

Deleted: ¶

595 cores of 19.41 (\pm 4.42) Mg C ha⁻¹. Over the full 50 cm, we estimate an OC stock of 32 (\pm 4.18) Mg C
 596 ha⁻¹ across all the cores (Table 3).

597 In order to estimate annual OC accumulation, the 50 cm stock (3,200 g C m⁻²) was divided by the
 598 approximate age of the 50 cm horizon. Considering a median sediment accretion rate of 8.54 cm kyr⁻¹,
 599 annual OC accumulation is estimated at 0.546 g C m⁻² yr⁻¹. These estimates should be treated with
 600 caution, bearing in mind that the sediment cores were extracted from the points of greatest sediment
 601 accumulation (Fig. 2). Furthermore, this also assumes a constant sediment accumulation over time and
 602 does not account for potential hiatuses or erosional activity, thus representative of a long-term historical
 603 estimate rather than flux.

604 The molar C/N ratios were used to assess the origin and degree of degradation of the organic matter. The
 605 average C/N ratio across all samples was 10.71 (\pm 3.19), with the highest value being 18.51 (V11) and the
 606 lowest value being 7.71 (V4).

Core	Avg C Density (kg C m ⁻³)	Carbon Stock Top 30 cm (Mg C ha ⁻¹)	Carbon Stock 50 cm (Mg C ha ⁻¹)
V1	5.87	24.28	29.36
V2	6.77	19.94	33.84
V4	7.75	14.92	31.31
V5	7.15	25.19	35.75
V6	6.54	20.68	61.4
V10	5.46	18.99	61.5
V11	5.031	11.82	61.7
All Cores	6.41	19.41	32.04

610 (V4) indicating
 611 predominantly marine sources.

Table 3. Summary table showing the average organic carbon density, the stock over the top 30 and 50 cm of the cores.

Deleted: carbon

Deleted: organic carbon

Formatted: English (UK)

Formatted Table

Formatted: English (UK)

Formatted: English (UK)

Formatted: English (UK)

Formatted: English (UK)

Formatted: English (UK)

Formatted: English (UK)

Moved (insertion) [3]

Formatted Table

Formatted: English (UK)

Formatted: English (UK)

Deleted: and the total length

619

620

621

622

623

624

625

635 Mixed-effects modelling indicated that OC density in the upper 50 cm was primarily explained by
 636 carbonate content and grain size (d50), with a weaker contribution from biogenic gravel content, while
 637 depth within the core showed no consistent effect. Alternative model structures, including sediment type,
 638 random slopes for depth, and AR(1) correlation across depth, did not improve model fit and were not
 639 retained (see Table A2, A3). In the final model, d50 was positively associated with OC density ($\beta = 0.177$,
 640 $p = 0.0046$) and carbonate was negatively associated with OC density ($\beta = -0.306$, $p < 0.001$), whereas
 641 biogenic gravel showed a weaker positive association ($\beta = 0.098$, $p = 0.0688$) and depth was not
 642 significant ($p = 0.577$). Approximately 42% of the variability in OC density was attributable to
 643 differences among cores, with the remaining variance occurring within cores and as unexplained residual
 644 variability (Fig. 5).

Deleted: organic carbon

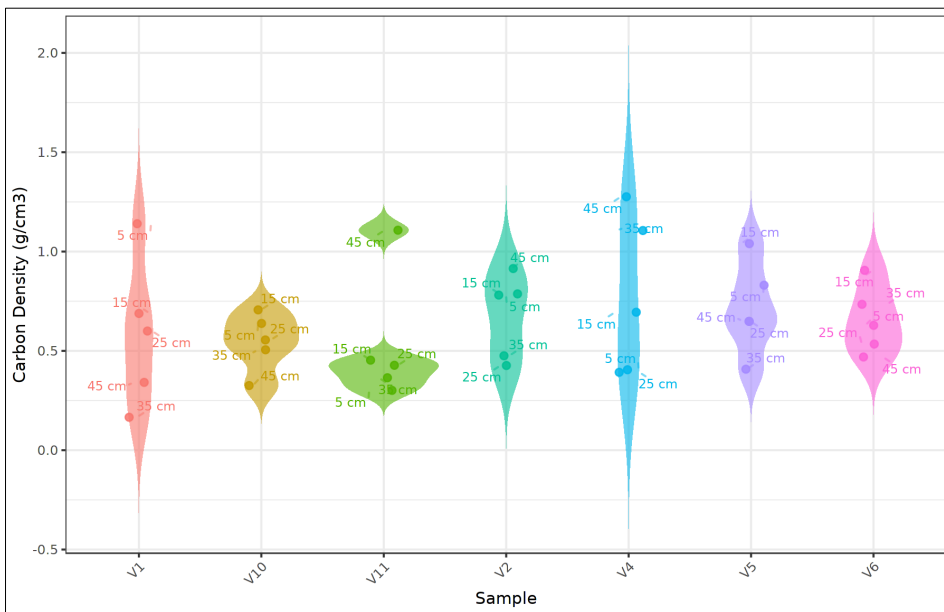
Deleted: supplementary t

Deleted: organic carbon

Deleted: organic carbon

Deleted: organic carbon

645



646

647 **Figure 5.** Organic carbon density in the sediments (g/cm^3) of the first 50 cm of cores.

Deleted: r

648

655 4. DISCUSSION

656 The Holocene sedimentary deposit underlying the present-day rhodolith bed in the Menorca Channel
657 reflects a highly dynamic environment shaped by post-glacial sea-level rise. The deposit rests on an
658 erosional unconformity that likely incorporates reworked Miocene–Pliocene materials (Guillén, 1987).
659 The pronounced spatial variability observed among corers, even over relatively short distances, suggests
660 that local paleo-topography has exerted a strong control on sediment accumulation. Similar patterns have
661 been reported from other temperate carbonate shelves, where interactions between seabed morphology
662 and hydrodynamic conditions generate a complex mosaic of erosion, transport and deposition (Betzler et
663 al., 2011; Fornós and Ahr, 1997). These processes have likely shaped the present bioclastic landscape of
664 the Menorca Channel and contributed to the long-term persistence of rhodolith-rich habitats. Importantly,
665 the heterogeneous distribution of sediments indicates that organic carbon storage is unlikely to be uni-
666 form across the bed. Consequently, reliable estimates of carbon stocks will require extending geophysical
667 surveys and sediment sampling to capture this spatial variability.

668 Radiocarbon data suggests that rhodolith assemblages in the Menorca Channel established during the
669 Early Holocene and developed under conditions comparable to other mid- to late-Holocene shallow ma-
670 rine carbonate systems. Their timing placed them between younger maërl deposits in western France
671 (5,860–5,300 yr BP, Ehrhold et al., 2021) and older rhodolith beds reported from the Gulf of Mexico
672 (13,886 yr BP, Olmstead and Andrus, 2024), although such comparisons should be interpreted cautiously
673 given regional differences in environmental and depositional settings. Within the Menorca Channel rec-
674 ords, sediment deposits formed at the end of the Younger Dryas and during rapid postglacial sea-level
675 rise (~9000 yr BP onwards) are characterized by bivalves-dominated assemblages with dispersed
676 branched rhodoliths. The interpretation of the lower and older sections of the cores is complicated by
677 evidence of reworked deposits; nevertheless, the data suggests that well-formed rhodoliths most probably
678 established later (upper ~60 cm of sediment, around 7,000–6,000 yr BP), with more stable marine con-
679 ditions, coinciding with sea-level stabilization near present-day levels (Lambeck, 1995). This transition
680 marks the onset of dense rhodolith beds characterised by large, tightly packed rhodoliths, with branched
681 and boxwork morphologies, whose expansion and long-term persistence were likely favoured by mod-
682 erate hydrodynamics, reduced terrigenous input, and mesophotic conditions that limit competitive pres-
683 sure (Aguirre et al., 2012; Basso et al., 2017). This continued presence over 6000 years highlights the
684 capacity of these systems to maintain structural complexity in the long-term, with potential implications
685 for their role as long-term organic carbon deposits, and for their conservation and management.

Deleted: is relatively thin and heterogeneous.

Formatted: Not Highlight

Deleted: Mapping sediment thickness was essential to re-
cover cores with sufficient depth to reconstruct the millen-
nial-scale depositional history of this ecosystem.

Deleted: indicate

Formatted: Not Highlight

Deleted: pre-date the large

Formatted: Not Highlight

Deleted: but are younger than the

Formatted: Not Highlight

Deleted: st

Deleted: s

Formatted: Not Highlight

Deleted: in

Formatted: Not Highlight

Formatted: Not Highlight

Deleted: , bearing in mind the

Formatted: Font: Not Bold

Deleted: Early Holocene

Deleted: and

Formatted: Not Highlight

Formatted: Not Highlight

Deleted: W

Deleted: including, in addition to

Deleted: and

Moved down [4]: Similar patchy and heterogeneous distribu-
tions have been reported in other deep Mediterranean rhodo-
lith beds (Bracchi et al., 2022; Rendina et al., 2020; Tabone et
al., 2024).

786 Present-day seafloor patterns in the Menorca Channel are characterized by patches of rhodoliths occur-
787 ring at high densities (50–100% surface coverage), ranging in size from ~10 m² to over 100 m², and
788 predominantly composed of branched forms (Cabrito et al., 2024a, b). This spatial heterogeneity is con-
789 sistent with observations from other deep Mediterranean rhodolith beds (Rendina et al., 2020; Bracchi et
790 al., 2022; Tabone et al., 2024). Sediments are consistently carbonate-rich and dominated by bioclastic
791 material, with relatively uniform organic carbon content in the upper layers. In contrast, sediment thick-
792 ness is highly heterogeneous at small spatial scales. Reflecting these patterns, mixed-effects modelling
793 indicated that approximately 42% of the variability in organic carbon density was attributable to differ-
794 ences among cores, suggesting small-scale patchiness in carbon accumulation across the rhodolith bed
795 that may be linked to local patchiness in rhodolith morphology and accumulation. Spatial heterogeneity,
796 together with variability in rhodolith density and morphology, may influence particle trapping capacity
797 and organic carbon retention (Cabrito et al., 2024a; Neto et al., 2021); however, this remains to be eval-
798 uated, as the cores analysed were collected in the deepest sediment deposits from the main rhodolith
799 patch characterized by high cover and structural complexity. Organic carbon density was largely con-
800 trolled by sediment composition (grain size and carbonate content), consistent with dilution in carbonate-
801 rich sediments and a textural control on carbon storage (Howard et al., 2018; Keil et al., 1994). The
802 absence of a depth effect suggests relatively uniform near-surface conditions, consistent with active bio-
803 turbation and hydrodynamic reworking that promote sediment mixing.

804 The relatively uniform organic carbon content in the upper 50 cm of sediment suggests low degradation
805 rates over the last ~6,000 years, coinciding with sea level stabilization. This stability likely favored the
806 development of well-formed rhodolith ecosystems, facilitating organic carbon capture and long-term re-
807 tention. Based on our estimates, these sediments store approximately 32.04 Mg C ha⁻¹ in the upper 50
808 cm, with an average of 19.41 (± 4.42) Mg C ha⁻¹ in the upper 30 cm. Using an estimated sediment
809 accretion rate of 8.54 cm kyr⁻¹, this corresponds to an average organic carbon accumulation of ~0.546 g
810 C m⁻² yr⁻¹. These values exceed previous estimates reported for coralline algal beds in temperate coastal
811 environments. For example, Mao et al. (2020) reported average organic carbon stocks of 7.23 ± 1.30 Mg
812 C ha⁻¹ within the upper 25 cm and 12.28 ± 1.98 Mg C ha⁻¹ across the full depth of carbonate deposits
813 (~80 cm) in Scottish coastal rhodolith beds. The substantially higher carbon stocks observed in the Me-
814 norca deposit likely reflect differences in the environmental context: extending to mesophotic depths it
815 allows long-term depositional stability and slow sediment turnover. Rather than acting as a rapid carbon
816 sink, this system would serve as a millennial-scale carbon reservoir, preserving organic matter within a
817 very slowly forming carbonate matrix. Nevertheless, future work should investigate deeper sediment

Deleted: ¶

¶

Formatted: Not Highlight

Formatted: Not Highlight

¶

Formatted: Italian, Not Highlight

Formatted: Italian

¶

¶

Formatted: Not Highlight

¶

¶

¶

¶

¶

¶

¶

¶

¶

¶

¶

¶

¶

Deleted: ¶

Formatted: Not Highlight

Formatted: Not Highlight

Formatted: Not Highlight

Formatted: Not Highlight

Formatted: Not Highlight

Formatted: Not Highlight

Formatted: Not Highlight

Formatted: Not Highlight

Formatted: Not Highlight

Formatted: Not Highlight

Formatted: Not Highlight

Formatted: Not Highlight

Formatted: Not Highlight

884 layers (>50 cm), to determine the depth and age at which organic carbon mineralized. This would also
885 help to clarify the role of spatial heterogeneity in the deposit, and whether areas with thinner sediment
886 cover differ in their capacity for carbon retention.

887 The relatively high organic carbon stocks documented in the Menorca Channel reinforce growing evi-
888 dence that rhodolith beds can contribute to long-term carbon storage despite their slow sediment accre-
889 tion rates (Mao et al., 2024; Van Der Heijden and Kamenos, 2015). The persistence of organic carbon
890 observed in these deposits reflects two complementary processes: the long-term preservation of organic
891 matter within slowly accumulating sediments and the longevity of coralline algal systems, whose car-
892 bonate skeletons resist degradation and maintain biogenic habitats over millennial timescales (Aguirre et
893 al., 2000; Van Der Heijden and Kamenos, 2015; Wilson et al., 2004). The three-dimensional structure of
894 rhodolith beds promotes the trapping and burial of suspended organic matter, including allochthonous
895 carbon, while low remineralization rates favour its preservation over long timescales (James et al.,
896 2024b). While rhodolith beds can store substantial amounts of organic carbon, their net contribution to
897 climate mitigation remains an open question because the balance between carbon burial and calcification-
898 related carbon release is not yet fully resolved (Kamenos et al., 2013; Mao et al., 2024; Schubert et al.,
899 2024; Van Der Heijden and Kamenos, 2015). Within this context, Blue Carbon frameworks have focused
900 on mangroves, salt marshes, and seagrass meadows. However, coralline algal beds are increasingly rec-
901 ognized as non-classical Blue Carbon ecosystems because of their capacity to store organic carbon over
902 centennial to millennial timescales (James et al., 2024a). While their annual accumulation rates are rela-
903 tively low, their extensive global distribution and long-term persistence suggest that their cumulative
904 contribution to coastal carbon storage may be substantial (Van Der Heijden and Kamenos, 2015). The
905 carbon stocks quantified in the Menorca Channel support this emerging perspective and highlight the
906 importance of protecting these ecosystems, as disturbance can rapidly mobilize carbon deposits that have
907 accumulated over millennia.

908 The extremely low sediment accretion rates make these organic carbon deposits highly vulnerable to
909 physical disturbance, particularly from bottom-contact fishing such as trawling and dredging (Trégarot
910 et al., 2024). These activities can fragment nodules, bury living rhodoliths, and alter the structure and
911 compaction of the sediment, with impacts that persist over timescales far longer than ecosystem man-
912 agement schemes (de Juan et al., 2013; Cabanellas-Reboredo et al., 2018; Tauran et al., 2020). The upper
913 few centimeters of the deposit can be disrupted by a single trawl passage, not only halting carbon seques-
914 tration but potentially remobilizing organic carbon that accumulated over thousands of years (Bernard et

Deleted: james

Deleted: and highlighting its ecological and climatic importance despite low annual productivity. Given their...

Deleted: slow

Deleted: ,

Deleted: are

Deleted: de Juan et al., 2013;

Deleted: ing

924 al., 2019). In the Mediterranean, many rhodolith beds remain exposed to such pressures, as they alternate
925 with soft-sediment ecosystems exposed to commercial trawling (de Juan et al., 2013; Illa-López et al.,
926 2023). In contrast, the Menorca Channel deposit has been protected from trawling due to the historical
927 presence of submarine communication cables. Evidence from this less disturbed site suggests relatively
928 uniform carbon preservation and burial under natural, undisturbed conditions. This evidence highlights
929 the need for future research into rhodolith beds. In particular, this would include assessing whether or-
930 ganic carbon trapped by rhodolith beds, as opposed to carbon produced via rhodolith calcification, is
931 sequestered at rates that balanced or exceed calcification-related carbon release. This highlights the crit-
932 ical role of protection in maintaining the long-term carbon storage and ecological integrity of rhodolith
933 ecosystems.

- Deleted: habitats
- Deleted: that overlap with
- Deleted: grounds
- Deleted: ; de Juan et al., 2013
- Deleted: largely
- Deleted: and its designation as a trawl-banned area since 2016
- Deleted: un-trawled
- Deleted: e
- Deleted: of potential organic carbon storage potential
- Deleted: stored in sediments
- Deleted: habitats

934 Conclusions

935 Rhodolith beds in the western Menorca Channel form the surficial sedimentary layer over a Holocene
936 depositional framework and constitute long-term sedimentary carbon archives within carbonate shelf
937 systems. Their organic carbon content remains relatively stable through the upper 50 cm, indicating sus-
938 tained accumulation and limited degradation over ~6,000 years. This persistence is enabled by the three-
939 dimensional structure of rhodoliths, which promotes sediment trapping and long-term carbon preserva-
940 tion despite slow accretion rates, supporting their role as long-term carbon reservoirs rather than rapid
941 carbon sinks. These systems have persisted despite environmental changes, including human impacts,
942 yet their slow growth and sensitivity to physical disturbance make them highly vulnerable. Protecting
943 rhodolith beds from trawling and dredging is essential not only for biodiversity conservation but also for
944 maintaining their function as long-term carbon stores and reinforcing their contribution to climate regu-
945 lation. These findings suggest that carbonate biogenic systems such as rhodolith beds should be recon-
946 sidered as long-term carbon repositories within blue carbon frameworks.

- Deleted: millennia-old sediments in the western Menorca Channel,
- Deleted: representing persistent carbon stocks during the Holocene, with with o
- Deleted: averaging 0.57% in
- Deleted: and showing minimal
- Deleted: Although sediment accretion is slow (median 8.54 cm kyr⁻¹),
- Deleted: create a stable matrix that traps and preserves carbon over millennial timescales, highlighting
- Deleted: beds
- Deleted: and environmental changes, actively storing carbon over millennia, and globally, calcified rhodolith deposits are stable over geological timescales. Given
- Deleted: vulnerability
- Deleted: ,
- Deleted: p
- Deleted: on
- Deleted: or
- Deleted: . Conserving rhodolith beds supports
- Deleted: ,
- Deleted: ecosystem resilience, and climate mitigation
- Deleted: . emphasizing their often-overlooked contribution to long-term carbon storage

947 Author contributions

948 SdJ, FM, and CL conceptualized the study. AC, MdMG, SdJ, RS, and LI conducted sample collection
949 and processing. MdMG and CL curated the data. SdJ, RS, and AO performed the formal analysis. CL,
950 RS, and AO developed the methodology. SdJ, FM, and CL prepared the original draft of the manuscript.
951 HH, JG, and GC contributed to reviewing and editing the manuscript. SdJ, FM, and GC acquired funding.

952 Competing interests

953 The authors declare that they have no conflict of interest.

990 **Code and data availability**

991 The data supporting the findings of this study, including sediment core descriptions, geochemical
992 analyses, and radiocarbon dates, are available from the corresponding author upon reasonable request.

Formatted: Font: Not Bold

Formatted: Font: Not Bold

993 **Acknowledgements**

994 The authors would like to thank the crew of the R/V SOCIB and R/V Sarmiento de Gamboa during the
995 research cruises, partly funded by the Spanish Ministry of Science and Innovation. We thank the compa-
996 nies NAUTILUS and GEOMY TSA for their technical support during field work to obtain geophysical
997 maps and vibrocores.

998 **Financial Support**

999 This work was funded by EU Horizon project MARBEFES (contract no. 101060937) and RHODOMED
1000 (Spanish Ministry of Science grant nº PID2023-146998OB-C22). This work contributes to IMEDEA's
1001 'Center of Excellence' Maria de Maetzu (CEX2021-001198) and ICM's 'Center of Excellence' Severo
1002 Ochoa (CEX2019-000928-5). The Spanish Ministry of Science and Innovation supported S.d.J. with a
1003 "Ramón y Cajal" grant (RyC2020-029062-I), A.O.-A. with a "Ramon y Cajal" grant (RyC2023-043454-
1004 I) and L.I.-L with a FPI predoctoral (PRE2022-104567).

1005 **References**

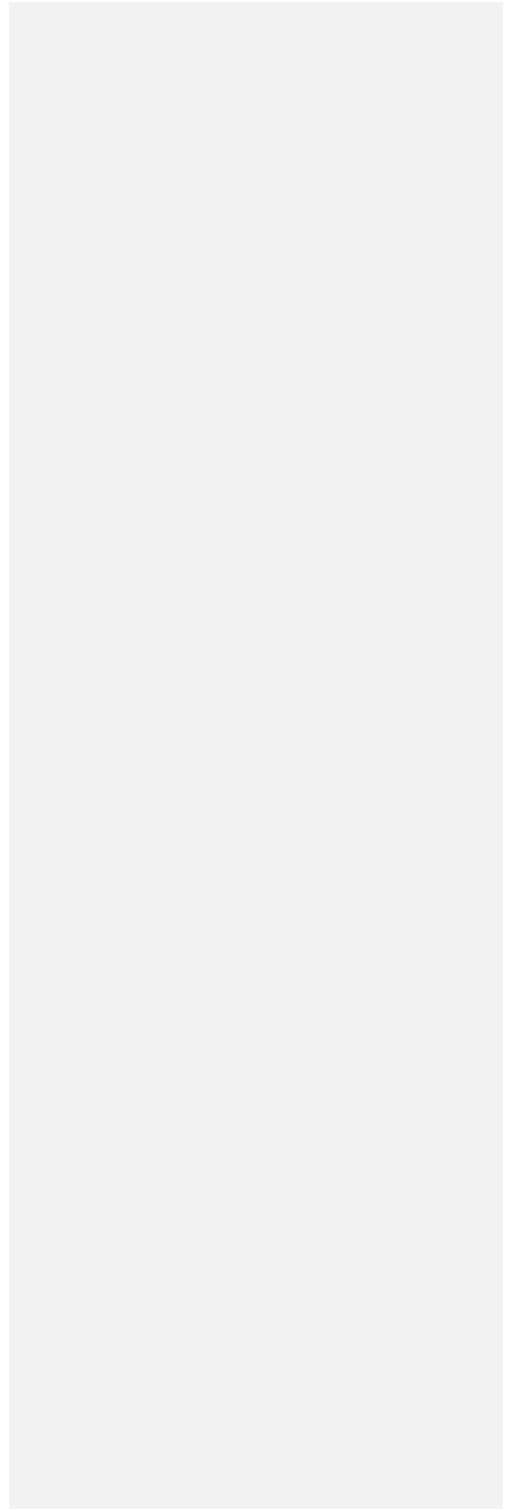
- 1006 Aguirre, J., Riding, R., and Braga, J. C.: Diversity of coralline red algae: origination and extinction
1007 patterns from the Early Cretaceous to the Pleistocene, *Paleobiology*, 26, 651–667, 2000.
- 1008 Aguirre, J., Braga, J. C., Martín, J. M., and Betzler, C.: Palaeoenvironmental and stratigraphic
1009 significance of Pliocene rhodolith beds and coralline algal bioconstructions from the Carboneras Basin
1010 (SE Spain), *Geodiversitas*, 34, 115–136, 2012.
- 1011 Aguirre, J., Braga, J. C., and Bassi, D.: Rhodoliths and rhodolith beds in the rock record, in:
1012 *Rhodolith/maërl beds: A global perspective*, Springer, 105–138, 2017.
- 1013 Alonso, B., Guillén, J., Canals, M., Serra, J., Acosta, J., Herranz, P., Sanz, J. L., Calafat, A., and
1014 CATAFAU, A.: Los sedimentos de la plataforma continental balear, *Acta Geológica Hispánica*, 185–
1015 196, 1988.
- 1016 Amado-Filho, G. M., Moura, R. L., Bastos, A. C., Salgado, L. T., Sumida, P. Y., Guth, A. Z., Francini-
1017 Filho, R. B., Pereira-Filho, G. H., Abrantes, D. P., Brasileiro, P. S., Bahia, R. G., Leal, R. N., Kaufman,
1018 L., Kleypas, J. a, Farina, M., and Thompson, F. L.: Rhodolith beds are major CaCO₃ bio-factories in
1019 the tropical South West Atlantic., *PloS ONE*, 7, e35171, <https://doi.org/10.1371/journal.pone.0035171>,
1020 2012.
- 1021 Barbier, E. B., Hacker, S. D., Kennedy, C. J., Koch, E. W., Stier, A. C., and Silliman, B. R.: The value
1022 of estuarine and coastal ecosystem services, *Ecological Monographs*, 81, 169–193, 2011.

- 1023 Basso, D.: Deep rhodolith distribution in the Pontian Islands, Italy: a model for the paleoecology of a
1024 temperate sea, *Palaeogeography, palaeoclimatology, palaeoecology*, 137, 173–187, 1998.
- 1025 Basso, D., Caragnano, A., Benzoni, F., Rodondi, G., and others: Southern Sinai rhodoliths: facies,
1026 species composition, and growth rate (Red Sea, Egypt), in: *International rhodolith workshop*, 2012.
- 1027 Basso, D., Babbini, L., Ramos-Esplá, A. A., and Salomidi, M.: Mediterranean rhodolith beds,
1028 *Rhodolith/Maërl Beds: a global perspective*, 281–298, 2017.
- 1029 Bernard, G., Romero-Ramirez, A., Tauran, A., Pantalos, M., Deflandre, B., Grall, J., and Grémare, A.:
1030 Declining maerl vitality and habitat complexity across a dredging gradient: insights from in situ
1031 sediment profile imagery (SPI), *Scientific Reports*, 9, 16463, 2019.
- 1032 Betzler, C., Braga, J. C., JARAMILLO-VOGEL, D., Roemer, M., Huebscher, C., Schmiedl, G., and
1033 Lindhorst, S.: Late Pleistocene and Holocene cool-water carbonates of the Western Mediterranean Sea,
1034 *Sedimentology*, 58, 643–669, 2011.
- 1035 Bianchi, C. N., Morri, C., Chiantore, M., Montefalcone, M., Parravicini, V., Rovere, A., and others:
1036 Mediterranean Sea biodiversity between the legacy from the past and a future of change, *Life in the*
1037 *Mediterranean Sea: a look at habitat changes*, 1, 55, 2012.
- 1038 Bosence, D. W.: The occurrence and ecology of recent rhodoliths—a review, *Coated grains*, 225–242,
1039 1983.
- 1040 Bracchi, V. A., Caronni, S., Meroni, A. N., Burguett, E. G., Atzori, F., Cadoni, N., Marchese, F., and
1041 Basso, D.: Morphostructural characterization of the heterogeneous rhodolith bed at the marine
1042 protected area “capo carbonara”(Italy) and hydrodynamics, *Diversity*, 14, 51, 2022.
- 1043 Bulleri, F., Schubert, N., Hall-Spencer, J. M., Basso, D., Burdett, H. L., Francini-Filho, R. B., Grall, J.,
1044 Horta, P. A., Kamenos, N. A., Martin, S., and others: Positive species interactions structure rhodolith
1045 bed communities at a global scale, *Biological Reviews*, 100, 428–444, 2025.
- 1046 Cabanellas-Reboredo, M., Mallol, S., Barberá, C., Vergés, A., Díaz, D., and Goñi, R.: Morpho-
1047 demographic traits of two maërl-forming algae in beds with different depths and fishing histories.,
1048 *Aquatic Conservation*, 28, 2018.
- 1049 Cabrito, A., de Juan, S., Hinz, H., and Maynou, F.: Morphological insights into the three-dimensional
1050 complexity of rhodolith beds, *Marine Biology*, 171, 127, 2024a.
- 1051 Cabrito, A., Maynou, F., Simide, R., Mouillot, D., Lossent, J., and de Juan, S.: Non-extractive fish
1052 diversity assessment in Mediterranean rhodolith beds, *Aquatic Conservation: Marine and Freshwater*
1053 *Ecosystems*, 34, e4212, 2024b.
- 1054 Canals, M. and Ballesteros, E.: Production of carbonate particles by phytobenthic communities on the
1055 Mallorca-Menorca shelf, northwestern Mediterranean Sea, *Deep Sea Research Part II: Topical Studies*
1056 *in Oceanography*, 44, 611–629, 1997.
- 1057 Ehrhold, A., Jouet, G., Le Roy, P., Jorry, S. J., Grall, J., Reixach, T., Lambert, C., Gregoire, G., Goslin,
1058 J., Roubi, A., and others: Fossil maerl beds as coastal indicators of late Holocene palaeo-environmental

- 1059 evolution in the Bay of Brest (Western France), *Palaeogeography, Palaeoclimatology, Palaeoecology*,
1060 577, 110525, 2021.
- 1061 Fornós, J. J. and Ahr, W.: Temperate carbonates on a modern, low-energy, isolated ramp; the Balearic
1062 platform, Spain, *Journal of Sedimentary Research*, 67, 364–373, 1997.
- 1063 Guillén, J.: La sedimentación carbonatada en la plataforma continental de Campos (Sur de Mallorca),
1064 1987.
- 1065 Howard, J. L., Creed, J. C., Aguiar, M. V., and Fourqurean, J. W.: CO₂ released by carbonate sediment
1066 production in some coastal areas may offset the benefits of seagrass “Blue Carbon” storage, *Limnology*
1067 and *Oceanography*, 63, 160–172, 2018.
- 1068 Illa-López, L., Cabrito, A., de Juan, S., Maynou, F., and Demestre, M.: Distribution of rhodolith beds
1069 and their functional biodiversity characterisation using ROV images in the western Mediterranean Sea,
1070 *Science of the Total Environment*, 905, 167270, 2023.
- 1071 James, K., Macreadie, P. I., Burdett, H. L., Davies, I., and Kamenos, N. A.: It’s time to broaden what
1072 we consider a ‘blue carbon ecosystem,’ *Global Change Biology*, 30, e17261, 2024a.
- 1073 James, K., Macreadie, P. I., Burdett, H. L., Davies, I., and Kamenos, N. A.: It’s time to broaden what
1074 we consider a ‘blue carbon ecosystem,’ *Global Change Biology*, 30, e17261, 2024b.
- 1075 Jardim, V. L., Grall, J., Barros-Barreto, M. B., Bizien, A., Benoit, T., Braga, J. C., Brodie, J., Burel, T.,
1076 Cabrito, A., Diaz-Pulido, G., and others: A common terminology to unify research and conservation of
1077 coralline algae and the habitats they create, *Aquatic Conservation: Marine and Freshwater Ecosystems*,
1078 35, e70121, 2025.
- 1079 Joher, S., Ballesteros, E., and Rodríguez-Prieto, C.: Macroalgal-dominated coastal detritic communities
1080 from the Western Mediterranean and the Northeastern Atlantic, *Mediterranean Marine Science*, 17,
1081 476–495, 2016.
- 1082 de Juan, S., Lo Iacono, C., and Demestre, M.: Benthic habitat characterisation of soft-bottom
1083 continental shelves: Integration of acoustic surveys, benthic samples and trawling disturbance intensity,
1084 *Estuarine, Coastal and Shelf Science*, 117, 199–209, <https://doi.org/10.1016/j.ecss.2012.11.012>, 2013.
- 1085 de Juan, S., Ospina-Alvarez, A., Hinz, H., Moranta, J., and Barberá, C.: The continental shelf seascape:
1086 a network of species and habitats, *Biodiversity and Conservation*, 1–20, 2023.
- 1087 Kamenos, N. A., Burdett, H. L., Aloisio, E., Findlay, H. S., Martin, S., Longbone, C., Dunn, J.,
1088 Widdicombe, S., and Calosi, P.: Coralline algal structure is more sensitive to rate, rather than the
1089 magnitude, of ocean acidification, *Global Change Biology*, 19, 3621–3628, 2013.
- 1090 Keil, R. G., Tsamakis, E., Fuh, C. B., Giddings, J. C., and Hedges, J. I.: Mineralogical and textural
1091 controls on the organic composition of coastal marine sediments: Hydrodynamic separation using
1092 SPLITT-fractionation, *Geochimica et Cosmochimica Acta*, 58, 879–893, 1994.
- 1093 Lambeck, K.: Late Pleistocene and Holocene sea-level change in Greece and south-western Turkey: a
1094 separation of eustatic, isostatic and tectonic contributions, *Geophysical Journal International*, 122,
1095 1022–1044, 1995.

- 1096 Lambeck, K. and Bard, E.: Sea-level change along the French Mediterranean coast for the past 30 000
1097 years, *Earth and Planetary Science Letters*, 175, 203–222, 2000.
- 1098 Lo Iacono, C., Mateo, M. A., Gracia, E., Guasch, L., Carbonell, R., Serrano, L., Serrano, O., and
1099 Danobeitia, J.: Very high-resolution seismo-acoustic imaging of seagrass meadows (Mediterranean
1100 Sea): Implications for carbon sink estimates, *Geophysical Research Letters*, 35, 2008.
- 1101 de Macêdo Carneiro, P. B., de Lima, J. P., Bandeira, Ê. V. P., Neto, A. R. X., Barreira, C. de A. R., de
1102 Souza Tâmega, F. T., Matthews-Cascon, H., Junior, W. F., and de Morais, J. O.: Structure, growth and
1103 CaCO₃ production in a shallow rhodolith bed from a highly energetic siliciclastic-carbonate coast in
1104 the equatorial SW Atlantic Ocean, *Marine environmental research*, 166, 105280, 2021.
- 1105 Macreadie, P. I., Anton, A., Raven, J. A., Beaumont, N., Connolly, R. M., Friess, D. A., Kelleway, J. J.,
1106 Kennedy, H., Kuwae, T., Lavery, P. S., and others: The future of Blue Carbon science, *Nature
1107 communications*, 10, 3998, 2019.
- 1108 Mao, J., Burdett, H. L., McGill, R. A., Newton, J., Gulliver, P., and Kamenos, N. A.: Carbon burial over
1109 the last four millennia is regulated by both climatic and land use change, *Global Change Biology*, 26,
1110 2496–2504, 2020.
- 1111 Mao, J., Burdett, H., and Kamenos, N.: Efficient carbon recycling between calcification and
1112 photosynthesis in red coralline algae, *Biology Letters*, 20, 2024.
- 1113 Middelburg, J. J.: Reviews and syntheses: to the bottom of carbon processing at the seafloor,
1114 *Biogeosciences*, 15, 413–427, 2018.
- 1115 Moranta, J., Barberá, C., Druet, M., and Zaragoza, N.: Caracterización ecológica de la plataforma
1116 continental (50-100 m) del canal de Menorca. Informe final área LIFE+ INDEMARES
1117 (LIFE07/NAT/E/000732), Instituto Español de Oceanografía-Centro Oceanográfico de Baleares
1118 (Palma), 2014.
- 1119 Nellemann, C. and Corcoran, E.: Blue carbon: the role of healthy oceans in binding carbon: a rapid
1120 response assessment, *UNEP/Earthprint*, 2009.
- 1121 Neto, J. M., Bernardino, A. F., and Netto, S. A.: Rhodolith density influences sedimentary organic
1122 matter quantity and biochemical composition, and nematode diversity, *Marine Environmental
1123 Research*, 171, 105470, 2021.
- 1124 Olmstead, S. A. and Andrus, C. F. T.: Growth characterization of mesophotic rhodoliths in the northern
1125 Gulf of Mexico using radiocarbon dating, *Palaeogeography, Palaeoclimatology, Palaeoecology*, 654,
1126 112438, 2024.
- 1127 Rendina, F., Kaleb, S., Caragnano, A., Ferrigno, F., Appolloni, L., Donnarumma, L., Russo, G. F.,
1128 Sandulli, R., Roviello, V., and Falace, A.: Distribution and characterization of deep rhodolith beds off
1129 the Campania coast (SW Italy, Mediterranean Sea), *Plants*, 9, 985, 2020.
- 1130 Rendina, F., Donnarumma, L., Ferrigno, F., and Russo, G. F.: Biodiversity of Mediterranean
1131 mesophotic rhodolith beds: Macrofaunal community composition and structure (SW Italy), *Continental
1132 Shelf Research*, 105682, 2026.

- 1133 Riosmena-Rodríguez, R., Nelson, W., and Aguirre, J.: Rhodolith/maërl beds: a global perspective,
1134 Springer, 2017.
- 1135 Schubert, N., Tuya, F., Peña, V., Horta, P. A., Salazar, V. W., Neves, P., Ribeiro, C., Otero-Ferrer, F.,
1136 Espino, F., Schoenrock, K., and others: “Pink power”—the importance of coralline algal beds in the
1137 oceanic carbon cycle, *Nature Communications*, 15, 8282, 2024.
- 1138 Tabone, L., Knittweis, L., Aguilar, R., Alvarez, H., Borg, J. A., Garcia, S., Schembri, P. J., and Evans,
1139 J.: Habitat characterization, anthropogenic impacts and conservation of rhodolith beds off southeastern
1140 Malta, *Aquatic Conservation: Marine and Freshwater Ecosystems*, 34, e4148, 2024.
- 1141 Tauran, A., Dubreuil, J., Guyonnet, B., and Grall, J.: Impact of fishing gears and fishing intensities on
1142 maerl beds: An experimental approach, *Journal of Experimental Marine Biology and Ecology*, 533,
1143 151472, 2020.
- 1144 Teichert, S.: Attached and free-living crustose coralline algae and their functional traits in the
1145 geological record and today, *Facies*, 70, 8, 2024.
- 1146 Trégarot, E., D’Olive, J. P., Botelho, A. Z., Cabrito, A., Cardoso, G. O., Casal, G., Cornet, C. C., Cragg,
1147 S. M., Degia, A. K., Fredriksen, S., and others: Effects of climate change on marine coastal
1148 ecosystems—A review to guide research and management, *Biological Conservation*, 289, 110394, 2024.
- 1149 Tuya, F., Schubert, N., Aguirre, J., Basso, D., Bastos, E. O., Berchez, F., Bernardino, A. F., Bosch, N.
1150 E., Burdett, H. L., Espino, F., and others: Levelling-up rhodolith-bed science to address global-scale
1151 conservation challenges, *Science of The Total Environment*, 164818, 2023.
- 1152 Van der Heijden, L. and Kamenos, N.: Calculating the global contribution of coralline algae to carbon
1153 burial, *Biogeosciences*, 12, 7845–7877, 2015.
- 1154 Van Der Heijden, L. and Kamenos, N. A.: Reviews and syntheses: calculating the global contribution of
1155 coralline algae to total carbon burial, *Biogeosciences*, 12, 6429–6441, 2015.
- 1156 Wilson, S., Blake, C., Berges, J. A., and Maggs, C. A.: Environmental tolerances of free-living coralline
1157 algae (maerl): implications for European marine conservation, *Biological conservation*, 120, 279–289,
1158 2004.
- 1159
- 1160
- 1161
- 1162



Page 3: [1] Deleted **Silvia de Juan** **10/04/2026 12:25:00**

▼
▲

Page 3: [2] Deleted **Ryan Smazal** **24/04/2026 14:38:00**

▼
▲

Page 3: [3] Deleted **Silvia de Juan** **10/04/2026 13:57:00**

▼
▲

Page 3: [4] Deleted **Silvia de Juan** **30/04/2026 09:55:00**

▼
▲

Page 3: [5] Deleted **Silvia de Juan** **30/04/2026 10:12:00**

▼
▲

Page 3: [6] Commented [GC7] **Grace Cott** **29/04/2026 13:21:00**

I think this is good and should be kept - it outlines the focus nicely

Page 3: [7] Deleted **Silvia de Juan** **10/04/2026 13:29:00**

▼
▲